CD36 coordinates NLRP3 inflammasome activation by facilitating the intracellular nucleation from soluble to particulate ligands in sterile inflammation

Published in final edited form as:
Nat Immunol. 2013 August ; 14(8): 812–820. doi:10.1038/ni.2639.

CD36 coordinates NLRP3 inflammasome activation by facilitating the intracellular nucleation from soluble to particulate ligands in sterile inflammation

Frederick J. Sheedy[1], **Alena Grebe**[2], **Katey J. Rayner**[1], **Parisa Kalantari**[3], **Bhama Ramkhelawon**[1], **Susan B. Carpenter**[3], **Christine E. Becker**[4], **Hasini N. Ediriweera**[1], **Adam E. Mullick**[5], **Douglas T. Golenbock**[3], **Lynda M. Stuart**[4], **Eicke Latz**[2,3,6], **Katherine A. Fitzgerald**[3], and **Kathryn J. Moore**[1]

[1]Department of Medicine, Marc and Ruti Bell Program for Vascular Biology and Disease, The Leon H. Charney Division of Cardiology, New York University School of Medicine, New York, NY, USA

[2]Institute of Innate Immunity, University of Bonn, Bonn, Germany

[3]Department of Infectious Diseases and Immunology, University of Massachusetts Medical School, Worcester, MA, USA

[4]Laboratory of Developmental Immunology, Department of Pediatrics, Massachusetts General Hospital, Harvard Medical School, Boston, MA, USA

[5]Isis Pharmaceuticals, Carlsbad, CA, USA

[6] German Center for Neurodegenerative Diseases (DZNE), Bonn, Germany.

Abstract

Particulate ligands including cholesterol crystals and amyloid fibrils induce NLRP3-dependent production of interleukin-1β (IL-1β) in atherosclerosis, Alzheimer's disease and diabetes. Soluble endogenous ligands including oxidized-LDL, amyloid-β and amylin peptides accumulate in these diseases. Here we identify a CD36-mediated endocytic pathway that coordinates the intracellular conversion of these soluble ligands to crystals or fibrils, resulting in lysosomal disruption and NLRP3-inflammasome activation. Consequently, macrophages lacking CD36 failed to elicit IL-1β production in response to these ligands and targeting CD36 in atherosclerotic mice reduced serum IL-1β and plaque cholesterol crystal accumulation. Collectively, these findings highlight the importance of CD36 in the accrual and nucleation of NLRP3 ligands from within the macrophage and position CD36 as a central regulator of inflammasome activation in sterile inflammation.

Interleukin-1β (IL-1β) has been linked to the pathogenesis of several sterile inflammatory diseases including atherosclerosis, type 2 diabetes (T2D) and Alzheimer's disease (AD). In each of these conditions, the accumulation of particulate materials at sites of inflammation -

Correspondence should be addressed to K.J.M. (Kathryn.Moore@nyumc.edu) Telephone: +1-212-263-9498.

AUTHOR CONTRIBUTIONS

FJS designed, performed and analyzed experiments. AG analyzed cholesterol crystals in atherosclerotic plaques, KJR and HNE assisted with mouse atherosclerosis experiments. PK, BR, SBC and CEB assisted with microscopy experiments. AEM provided CD36 antisense oligonucleotides and contributed to experimental design. DTG, LMS, EL, and KAF contributed to study design, data analysis, and manuscript preparation. KJM conceived the study, designed and analyzed experiments, and prepared the manuscript with FJS.

COMPETING FINANCIAL INTERESTS

AEM is an employee of Isis Pharmaceuticals, a biotechnology company developing anti-sense oligonucleotide therapies.

cholesterol crystals in sub-endothelial spaces of atherosclerotic plaques[1], fibrillar amyloid-β (fAβ) in senile AD plaques[2], or amyloid-containing amylin/islet amyloid polypeptide (IAPP) on pancreatic β-cells in T2D[3] – is a hallmark of disease. Recent studies have identified these particulate endogenous ligands as activators of inflammasomes formed by the cytoplasmic sensor NLRP3 (refs. 4, 5, 6, 7). The NLRP3-inflammasome complex regulates activation of caspase-1, which catalyzes the cleavage of pro-IL-1β and pro-IL-18 (ref. 8), and promotes the secretion of these now biologically active cytokines as well as IL-1α[9]. However, the mechanisms by which such structurally distinct molecules activate the NLRP3 inflammasome remain elusive.

Full activation of the NLRP3 inflammasome in macrophages requires two steps: "priming" (signal 1) and activation of inflammasome complex assembly (signal 2). Priming of macrophages increases expression of both pro-IL-1β and NLRP3 (refs. 10, 11, 12), and can be achieved *in vitro* through ligation of the Toll-like receptors (TLRs). Thus, experimental studies typically use bacterial products to prime the NLRP3 inflammasome, as the nature of the immunostimulatory priming signals found in atherosclerosis, AD and T2D are not well described. Signal 2 appears to be triggered by perturbation of cytoplasmic homeostasis due to 'lysosomal destabilization'[13]. This process, triggered by certain aggregated and insoluble materials, is characterized by the cytosolic release of lysosomal contents[13] (eg. cathepsins) and/or reactive oxygen species (ROS)[14], which results in NLRP3 inflammasome assembly and caspase-1 activation. Whether signal 1 and signal 2 are unrelated *in vivo* or whether common molecular events underlie these apparently distinct processes remains undefined.

The mechanisms controlling the generation of NLRP3-activators in atherosclerosis, T2D and AD are not well understood. For example, the deposition of cholesterol-rich lipoproteins in the vessel wall is a key pathogenic step in atherosclerosis[15], yet the origin of cholesterol crystals which accumulate in plaques[1] is poorly understood. Recent studies using combined confocal-reflection microscopy revealed that crystals are present in early plaques, both in extracellular spaces and within macrophages[4, 16]. In the AD brain and diabetic pancreas, amyloid plaques arise from the aggregation of pre-fibrillar amyloidogenic peptides such as the Aβ(1-42) peptide[17, 18, 19] or IAPP[20, 21, 22], which oligomerize and give rise to higher order structures, including fibrils. Extracellular deposits of IAPP-amyloid in the pancreas of T2D diabetic subjects are associated with loss of insulin-producing β-cells, and amyloid is also detected within pancreatic macrophages which secrete IL-1β[23, 24]. Similarly, fAβ peptides accumulate in extracellular plaques in the AD brain, and increasing evidence indicates that soluble forms of Aβ are also damaging[25, 26]. The current paradigm suggests that the immunostimulatory aggregates of these NLRP3 agonists form in the extracellular space, and that their engulfment by macrophages triggers a process of dysfunctional phagocytosis or lysosomal damage that activates the NLRP3-inflammasome and the release of IL-1 family cytokines.

CD36 is an archetypal pattern recognition receptor that binds polyanionic ligands of both pathogen and self-origin[27], and is implicated in the pathogenesis of atherosclerosis and AD through its recognition of modified endogenous ligands, including oxidized LDL (oxLDL)[28], fAβ[29], and soluble Aβ (sAβ)[30]. CD36 cooperates with a TLR heterodimer of TLR4-TLR6 to recognize oxLDL and fAβ, and induce the inflammatory response to these endogenous ligands[31]. Mice lacking CD36 (*Cd36*$^{-/-}$) mice are protected from the toxic effects of fAβ[32], atherosclerosis[33, 34], insulin resistance and obesity[35, 36, 37]. These observations prompted us to investigate the role of CD36 in inflammasome priming and activation in atherosclerosis, T2D and AD. We show herein that in response to oxLDL, CD36 initiated both signal 1 and signal 2 for complete activation of the NLRP3 inflammasome: CD36 cooperated with TLR4-TLR6 to prime the NLRP3 inflammasome, and its unabated uptake of oxLDL, characteristic of scavenger receptors, resulted in the

formation of intracellular cholesterol crystals that caused lysosomal destabilization and NLRP3 activation. We extended this example of NLRP3 activation by particulate ligands formed from within the cell by showing that CD36 also regulated uptake of pre-fibrillar soluble Aβ and IAPP peptides that were transformed in the lysosome to thioflavin-reactive amyloid that triggered NLRP3. Collectively, our results suggest a new model of lysosomal-mediated NLRP3 activation that occurs from within after *de novo* aggregation and transformation of the soluble ligands into their pathogenic form. Furthermore, these studies identify CD36 ligation as the common molecular event that links sterile ligand recognition with NLRP3 inflammasome priming and activation in atherosclerosis, AD and T2D.

RESULTS

CD36 uptake of oxLDL generates NLRP3-activating crystals

Oxidized LDL is a key inflammatory component of atherosclerotic plaques that contains oxidation-specific epitopes that share molecular identity with phosphorylcholine moieties present on *Streptococcus pneumoniae*[38]. Recognition of this “danger associated molecular pattern” (DAMP) by CD36 leads to oxLDL uptake by recruited monocytes and the formation of cholesterol-laden macrophage foams cells which establish the atherosclerotic lesion. Notably, oxLDL, but not unmodified LDL, induced the release of IL-1β from lipopolysaccharide (LPS)-primed wild-type, but not *Cd36*$^{-/-}$ macrophages (**Fig. 1a, left panel**). CD36 deficiency did not affect induction of IL-1β by other NLRP3 activators including cholesterol crystals generated *in vitro* or ATP, or the AIM2-inflammasome activator poly(dA:dT) (**Fig. 1a, right panel**). To understand how CD36-mediated uptake of oxLDL activates the NLRP3-inflammasome, we used combined confocal-reflection microscopy to monitor for crystalline material in macrophages. We observed a dose- and time-dependent increase in the appearance of crystals within macrophages treated with oxLDL, but not native LDL (**Fig. 1b, Supplementary Fig. 1**), and this was markedly reduced in similarly treated *Cd36*$^{-/-}$ macrophages (**Fig. 1b, Supplementary Fig. 1a**). Acetylated and minimally oxidized LDL, which bind SR-A and CD14 (but not CD36), also induced intracellular crystal formation, albeit to a lesser extent than oxLDL (**Supplementary Fig. 1b**). Treatment with methyl-β-cyclodextrin to deplete cells of cholesterol reversed the appearance of reflective material in oxLDL-treated macrophages confirming that this crystalline material was cholesterol (**Fig. 1c**). Although CD36 can act as a TLR4-TLR6 co-receptor, oxLDL-induced crystal formation was unimpeded in *Tlr4*$^{-/-}$ and *Tlr6*$^{-/-}$ macrophages, and oxLDL-induced IL-1β secretion from LPS-primed *Tlr6*$^{-/-}$ macrophages was similar to wild-type macrophages (**Supplementary Fig. 2a-b**). However, blocking CD36-mediated oxLDL endocytosis using cytochalasin-D inhibited both the formation of intracellular crystals and IL-1β secretion in LPS-primed macrophages (**Fig. 1d-e)**, whilst induction of IL-1β by ATP was unaffected (**Fig. 1e**). Notably, despite similar accumulation of crystals in oxLDL-treated wild-type and *Nlrp3*$^{-/-}$ macrophages (**Fig. 1f**), secretion of IL-1β was abrogated in *Nlrp3*$^{-/-}$ macrophages confirming the dependence of this response on the NLRP3 inflammasome (**Fig. 1g**). IL-1β was similarly reduced in *Nlrp3*$^{-/-}$ macrophages treated with other NLRP3-activators, including synthetic cholesterol crystals and ATP. Finally, oxLDL-induced IL-1β was dependent on caspase-1 as this response was reduced in LPS-primed macrophages treated with both a broad (ZVAD-fmk) or specific (YVAD-fmk) caspase-1 inhibitor peptide, which also inhibited IL-1β secretion induced by synthetic cholesterol crystals, ATP and AIM2 (**Fig. 1h**). These data establish CD36-regulated cholesterol crystal formation as a key driver of inflammasome activation upstream of NLRP3.

Lysosomes control crystal formation and NLRP3 activation

Unlike the LDL receptor, CD36 is downregulated by its ligands, leading to an unabated uptake of oxLDL and its cholesterol cargo[39]. To examine the subcellular localization and fate of oxLDL-induced crystals we used lysosomal tracers combined with confocal-reflection fluorescence microscopy. Upon treatment of wild-type macrophages with oxLDL, crystals appeared in acidic lysosomal compartments which stain with the lysomotropic-dye Lysotracker within 8 hours (**Fig. 2a**). Labeling of lysosomes by incubating macrophages with fluorescent dextran revealed that crystal-containing lysosomes began to destabilize over 24 hours, as seen by the translocation of dextran into the cytosol (**Fig. 2b**). Similarly treated *Cd36*$^{-/-}$ macrophages displayed a punctate perinuclear staining pattern characteristic of intact lysososomes, consistent with oxLDL-induced crystals being the source of the lysosomal damage (**Fig. 2a,b**). By contrast, treatment with pre-formed cholesterol crystals induced the release of lysosomal dextran to a similar extent in wild-type and *Cd36*$^{-/-}$ macrophages (**Fig. 2b**). Unmodified LDL did not disrupt macrophage lysosomal integrity (**Fig. 2b**). We confirmed these findings using a fluorescent Lysotracker flow-cytometry based assay in which lysosomal destabilization was quantified by the increase in Lysotracker-negative cells. Consistent with the fluorescence microscopy findings, synthetic crystalline cholesterol, but not unmodified LDL, increased the percentage of Lysotracker-negative cells in both wild-type and *Cd36*$^{-/-}$ macrophages. By contrast, oxLDL increased the Lysotracker-negative cell population in wild-type but not *Cd36*$^{-/-}$ macrophages (**Fig. 2c**). To further investigate the role of lysosomal function in oxLDL-triggered NLRP3 activation we inhibited macrophage lysosomal maturation using bafilomycin-A1 and observed a marked reduction in IL-1β secretion by macrophages treated with oxLDL or synthetic crystalline cholesterol, but not ATP or poly(dA:dT) (**Fig. 2d**). IL-1β inhibition was similarly observed in macrophages treated with a broad inhibitor of the serine/protease family of cathepsins, FA-fmK (**Supplementary Fig. 2c**), implicating the release of these lysosomal enzymes in NLRP3 activation by oxLDL. Bafilomycin-A1 also blocked the formation of cholesterol crystals by oxLDL (**Fig. 2e**), implicating lysosomal activity not just in transmission of the signal to NLRP3, but also in regulating lysosomal cholesterol crystallization. Lysosomal acidification is a key step that is blocked by bafilomycin-A1 and is required for the hydrolysis of cholesterol esters in oxLDL by lysosomal acid lipase (LAL) to free cholesterol, which is more readily crystallized. To test whether this catabolic event was required for cholesterol crystallization and NLRP3 activation, we treated macrophages with Lalistat, a specific inhibitor of LAL[40]. Lalistat abrogated cholesterol crystal formation within oxLDL-treated macrophages (**Fig. 2f**), as well as mature IL-1β secretion (**Fig. 2g**), but did not affect IL-1β secretion induced by *in vitro* formed cholesterol crystals. Together, these data support the existence of a model of NLRP3-activation distinct from that of "frustrated phagocytosis" of extracellular particulate materials, in which the unabated uptake of oxLDL by CD36 causes the nucleation and accrual NLRP3-activating crystals within the macrophage.

CD36 cooperates with TLR4-TLR6 to prime the inflammasome

The dual requirement for priming and activating signals for full NLRP3 activation functions as a safeguard against the accidental or uncontrolled release of IL-1β. During the course of our studies, we noted that oxLDL had the unusual ability to induce mature IL-1β from unprimed macrophages, a response dependent on CD36 (**Fig. 3a**). As Signal 1 often proceeds through TLRs, we investigated whether CD36 cooperative signaling with TLR4-TLR6 provides the oxLDL priming signal. Treatment of macrophages with oxLDL alone induced modest amounts of IL-1β which were not enhanced in the presence of the NLRP3-activator ATP (**Fig. 3a**), confirming that oxLDL can provide both signal 1 and 2 for NLRP3 activation. Notably, IL-1β production was impaired in *Cd36*$^{-/-}$, *Tlr4*$^{-/-}$ and *Tlr6*$^{-/-}$ macrophages, indicating that this heterotrimeric signaling complex was required for NLRP3

priming by oxLDL. Similar results were obtained when macrophages were primed with oxLDL, but cholesterol crystals were used as the NLRP3 activator (**Supplementary Fig. 2d**). Because of the modest IL-1β amounts detected when oxLDL was used as a priming agent, we employed macrophage-based fluorescent ASC (ASC-CFP) assay to further assess the role of oxLDL in priming NLRP3 (ref. 11). ASC-CFP is polydispersed throughout the cytoplasm in unstimulated macrophages, however supramolecular assembly of ASC occurs upon signal 1 and 2, as was seen in cells primed with LPS and subsequently treated with ATP (**Fig. 3b**, bottom left). Treatment with oxLDL alone induced the formation of ASC-complexes consistent with the notion that oxLDL not only primed, but also activated NLRP3. Treatment with ATP following oxLDL priming also induced the formation of speck-like complexes, albeit to a lower frequency than in LPS-primed cells (**Fig. 3b, c**).

CD36 primes the NLRP3 inflammasome *in vivo*

To explore the role of CD36, TLR4 and TLR6 in transducing the oxLDL priming signal, we measured the requirement of this signaling complex in the transcriptional induction of inflammasome substrates and NLRP3 itself. OxLDL, but not LDL, induced *Il1b* and *Il1a* mRNA in wild-type macrophages, whereas *Il18* mRNA was unchanged consistent with its high basal expression in macrophages (**Fig. 3d**, **Supplementary Fig. 3**). Furthermore, oxLDL-induced macrophage *Nlrp3* mRNA, a critical checkpoint in NLRP3 priming, but not *Nlrc4*, an NLR involved in bacterial recognition. Notably, induction of *Il1a, Il1b* and *Nlrp3* mRNA was not observed in *Cd36*$^{-/-}$, *Tlr4*$^{-/-}$ and *Tlr6*$^{-/-}$ macrophages treated with oxLDL (**Fig. 3d)**. Triggering of CD36-TLR4-TLR6 by oxLDL induced NF-κB activation and ROS[31], two signals required for effective priming of the NLRP3-inflammasome. Consistent with this, the induction of *Il1a, Il1b* and *Nlrp3* mRNA by oxLDL was inhibited by the IKKβ inhibitor BAY 11-7082 (**Fig. 3e**) and by the NADPH oxidase enzyme complex inhibitor DPI (**Fig. 3f**). These data indicate that CD36-TLR4-TLR6, acting via NF-κB and ROS, primes the NLRP3 inflammasome in response to oxLDL.

The endogenous NLRP3 priming signals in atherosclerosis remain unclear. We postulated that CD36 recognition of oxidized forms of LDL that accumulate during hypercholesterolemia can prime macrophages *in vivo*. To test this, we used an *in vivo* model of foam cell formation by isolating peritoneal macrophages from atherogenic *Apoe*$^{-/-}$ or *Cd36*$^{-/-}$*Apoe*$^{-/-}$ mice fed a western diet for 12 weeks. Macrophages isolated from western diet-fed *Apoe*$^{-/-}$ mice exhibit increased abundance of *Il1a, Il1b* and *Nlrp3* mRNA compared to macrophages from normolipidemic wild-type mice (**Fig. 3g**), indicating that these cells were '*in vivo* primed' for NLRP3 activity. This increase in NLRP3 priming signals was specific, as no differences in *Il18* or *Nlrc4* mRNA were detected. By contrast, macrophages from western diet-fed *Cd36*$^{-/-}$*Apoe*$^{-/-}$ mice exhibited comparable *Il1a, Il1b* and *Nlrp3* mRNA abundance to chow-fed mice. Furthermore, *ex vivo* treatment of macrophages from western diet-fed *Apoe*$^{-/-}$ mice with the NLRP3-activator ATP (signal 2) induced IL-1β secretion, whereas no increase in IL-1β secretion was detected in macrophages from similarly treated *Cd36*$^{-/-}$*Apoe*$^{-/-}$ mice (**Fig. 3h**). Moreover, secretion of IL-1α, a function dependent on the inflammasome, was similarly upregulated in macrophages from western diet-fed *Apoe*$^{-/-}$ but not *Cd36*$^{-/-}$*Apoe*$^{-/-}$ mice treated with ATP (**Fig. 3i**). These data demonstrate the requirement for CD36 in NLRP3 priming of macrophages by atherogenic stimuli *in vivo*.

Targeting CD36 reduces inflammasome activation *in vivo*

To further investigate the role of CD36 and its signaling partners TLR4-TLR6 in inflammasome priming and activation *in vivo*, we generated *Apoe*$^{-/-}$ mice deficient in CD36, TLR4 or TLR6 and fed them a western diet for 12 weeks. Despite similar concentrations of total cholesterol in all groups (**Supplementary Table 1)**, aortic plaque

formation was significantly reduced in *Cd36*$^{-/-}$*Apoe*$^{-/-}$, *Tlr4*$^{-/-}$ *Apoe*$^{-/-}$ and *Tlr6*$^{-/-}$*Apoe*$^{-/-}$ mice compared to *Apoe*$^{-/-}$ controls (**Fig. 4a, Supplementary Fig. 4**). These double knock-out mice also exhibited reduced concentrations of serum IL1β, IL1α and IL18 (**Fig. 4b**), as well as *Il1a, Il1b* and *Nlrp3* mRNA in the aorta, indicative of reduced inflammasome activity (**Fig. 4c**). Furthermore, measurement of cholesterol crystal accumulation in plaques using confocal reflection microscopy revealed a specific reduction in crystal burden in *Cd36*$^{-/-}$*Apoe*$^{-/-}$ mice (**Fig 4d-e**) supporting the hypothesis that CD36 regulates inflammasome activity during atherogenesis by modifying both signal 1 and signal 2. We also observed a decrease in plaque IL-1β and active caspase-1 fluorescent staining in *Cd36*$^{-/-}$*Apoe*$^{-/-}$, *Tlr4*$^{-/-}$*Apoe*$^{-/-}$ and *Tlr6*$^{-/-}$*Apoe*$^{-/-}$ mice compared to *Apoe*$^{-/-}$ controls (**Fig 4f**). Nevertheless, there was a greater reduction of caspase-1 and IL-1β in *Cd36*$^{-/-}$*Apoe*$^{-/-}$ compared with *Tlr4*$^{-/-}$*Apoe*$^{-/-}$ or *Tlr6*$^{-/-}$*Apoe*$^{-/-}$ plaques, consistent with a critical role for CD36 in both priming and activating the NLRP3 inflammasome. We next determined whether therapeutic targeting of CD36 using an anti-sense oligonucleotide (ASO), which potently inhibits CD36 expression in macrophages *in vitro* and *in vivo* (**Supplementary Fig. 5**), could prevent inflammasome activation in western diet-fed *Apoe*$^{-/-}$ mice. Notably, serum IL-1β increased in *Apoe*$^{-/-}$ mice receiving weekly injections of control-ASO, but not CD36-ASO, over 4 weeks (**Fig. 4g**).

CD36 regulates amyloid formation and NLRP3 activation

Like atherosclerosis, AD is characterized by a protracted inflammatory response driven by cells of the monocyte lineage. fAβ activates the NLRP3 inflammasome and IL-1β secretion in LPS-primed macrophages and microglia[5], and a recent study demonstrated that NLRP3 activation contributes to AD[41]. We recently showed that CD36 binds to soluble (pre-fibrillar) Aβ[30] prompting us to investigate whether CD36 uptake of this soluble ligand could also promote the intracellular generation of an NLRP3-activator. We treated macrophages with sAβ, which was confirmed to be non-fibrillar (**Supplementary Fig. 6a)**, and stained with thioflavin-S, a dye that becomes fluorescent upon binding amyloid oligomers and fibrils. Confocal microscopy revealed a time-dependent increase in the appearance of intracellular thioflavin-S fluorescence in wild-type but not *Cd36*$^{-/-}$ macrophages treated with sAβ (**Fig. 5a**). Macrophages incubated with the non-amyloidogenic reverse peptide (revAβ) revealed no evidence of thioflavin-S-reactivity for up to 24 h, whereas thioflavin-S-reactive amyloid was apparent in wild-type macrophages as early as 3h after addition of sAβ and localized to lysosomes (**Fig. 5a,b**). No extracellular or cell-associated fibrils were observed by confocal microscopy (**Fig. 5a, b**), and sAβ incubated at 37 °C in cell culture medium for up to 24 hours showed no evidence of thioflavin-T reactivity (**Supplementary Fig. 6b**). Over that time frame (3-24h), sAβ induced the progressive release of IL-1β when incubated with LPS-primed wild-type, but not *Nlrp3*$^{-/-}$ or *Ice*$^{-/-}$ (caspase-1 knock-out) macrophages, indicating that uptake of this soluble ligand resulted in NLRP3-activation (**Fig. 5c, Supplementary Fig. 6b, lower panel**). Of note, sAβ was as effective an NLRP3-activator as fAβ, and pretreating macrophages with Congo Red to interfere with β-sheet formation blocked IL-1β secretion (**Fig. 5d**). Finally, secretion of IL-1β by sAβ was abrogated in *Cd36*$^{-/-}$ macrophages, indicating the critical role of this receptor-mediated uptake pathway in the generation of intracellular NLRP3-activating amyloid (**Fig. 5e**).

Recent studies identified activation of the NLRP3-inflammasome by another amyloidogenic peptide, IAPP, as a mechanism for enhanced IL-1β in T2D[6]. Interestingly, IAPP peptides delivered to macrophages in a soluble form were preferential activators of NLRP3 (ref. 6). We postulated that CD36-mediated uptake of IAPP may promote intracellular amyloid formation and NLRP3-activation, as observed with sAβ. Binding of a fluorescently-labeled human IAPP peptide (FAM-IAPP) or HiLyte-tagged sAβ was increased in cells stably overexpressing CD36 (CHO-CD36) compared to control cells (CHO-eV) (**Fig. 6a**).

Furthermore, wild-type but not *Cd36*$^{-/-}$ macrophages incubated with soluble huIAPP showed a time-dependent increase in intracellular thioflavin-S fluorescence (**Fig. 6b**). No such increase in thioflavin-S staining was observed in macrophages treated for up to 24 hours with rat IAPP, which is non-amyloidogenic due to species-specific amino acid differences (**Fig. 6b**). The intracellular accumulation of thioflavin-S-reactive amyloid altered lysosomal stability, as wild-type macrophages treated with fluorescent dextran and incubated with huIAPP or sAβ for 24 h showed a loss of lysosomal integrity, evidenced by the leakage of dextran into the cytoplasm (**Fig. 6c**). Soluble IAPP induced the progressive release of IL-1β, from as early as 3h, when incubated with LPS-primed wild-type but not *Nlrp3*$^{-/-}$ or *Ice*$^{-/-}$ macrophages. (**Fig. 6d, Supplementary Fig. 6c**). By contrast, soluble IAPP incubated at 37°C in cell culture medium alone showed no evidence of thioflavin-T reactivity for up to 12 hours. Notably, the lysosomal damage induced by these amyloidogenic peptides, and subsequent IL-1β secretion, were abrogated in *Cd36*$^{-/-}$ macrophages (**Fig. 6c, e**). Furthermore, pre-treating macrophages with Congo Red blocked the accumulation of thioflavin-reactive IAPP and IL-1β secretion (**Fig. 6f**), indicating that the intracellular transformation of soluble IAPP resulted in NLRP3 activation. Moreover and consistent with what we observed with oxLDL-induced cholesterol crystals, phagolysosomal activity was required for NLRP3 activation by huIAPP and sAβ as pre-treatment with cytochalasin-D to block endocytosis, bafilomycin-A1 to block lysosomal acidification or FA-fmk to inhibit the serine/protease family of cathepsins, blunted IL-1β production (**Supplementary Fig. 6d-e**). These data support the existence of a common pathway through which CD36-mediated uptake of the soluble precursors of NLRP3 ligands facilitates the intracellular generation of pathogenic NLRP3 activators.

DISCUSSION

Our work here identifies CD36 as a master regulator of inflammasome activation in atherosclerosis, AD and T2D that facilitates the accrual and intralysosomal conversion of soluble endogenous ligands (oxLDL, sAβ and IAPP) to insoluble crystals or amyloid oligomers/fibrils and consequently, NLRP3 activation leading to IL-1β secretion. Lysosomal dysfunction plays a critical role in both the generation of crystalline and amyloid ligands, and the transmission of the damaging effects of these ligands sensed by NLRP3. Our results suggest a new model of NLRP3 activation by particulate ligands formed from within the macrophage, and place CD36 upstream of a common mechanism of NLRP3-dependent IL-1β secretion in several sterile inflammatory diseases.

In each of the diseases focused on in this study, the accumulation of particulate materials at sites of inflammation is a pathological hallmark. Unlike previously proposed models of NLRP3 activation in these diseases in which “frustrated phagocytosis” of extracellular particulate materials triggers the inflammasome[4, 5], our findings suggest that the earliest activation of NLRP3 by cholesterol crystals or Aβ/IAPP fibrils results from recognition and endocytosis of the soluble precursors of particulate ligands (eg. oxLDL, sAβ, sIAPP) by CD36 and the subsequent intracellular nucleation of insoluble NLRP3-activators. Our data fit with previous observations of intracellular amyloid fibril formation *in vitro*[23, 24, 25, 26, 42, 43], and an increasing literature that suggests that sAβ and sIAPP are the damaging species in AD and T2D, respectively. In addition to fibrillar forms of amyloid, macrophages incubated with sAβ and sIAPP may also contain higher order oligomeric forms of these peptides in the lysosome that may activate NLRP3. Whilst these studies do not exclude the possibility that extracellular crystals or amyloid fibrils exist which also activate the NLRP3 inflammasome through the ‘frustrated phagocytosis’ process, here we expand upon this paradigm by suggesting that such ligands may be secondary triggers of NLRP3 that arise later in disease due to their active export from macrophages or the release of crystals/fibrils from dying cells. Macrophage cell death may itself be triggered by

inflammasome activation through the process known as pyroptosis[44] which is linked to the release of pro-atherogenic IL1α[45, 46, 47], or as a result of lysosomal dysfunction due to the prolonged accumulation of insoluble crystals or fibrils.

In the case of atherosclerosis, CD36 plays a dual role in initiating both priming (signal 1) and activation (signal 2) of the NLRP3 inflammasome. Although oxLDL has been known to trigger IL-1β production in foam cells[48, 49, 50], many of these studies were carried out before identification of the NLRP3-inflammasome. Our work provides the molecular mechanism for how oxLDL induces macrophage secretion of IL-1β by showing that CD36 binding of this ligand controls its engagement of the two necessary pathways for full inflammasome activation: Signal 1 via the TLRs and Signal 2 via the NLRs. Whilst previous studies of inflammasome activity in host defense and inflammatory disease have suggested that signal 1 and signal 2 are derived from separate DAMPS engaging distinct signaling pathways, our data suggests that a single DAMP (oxLDL) provides both signals in atherosclerosis by engaging CD36. Whilst the amounts of priming signals induced by oxLDL via CD36-TLR4-TLR6 are modest compared to a bacterial stimuli it is consistent with atherosclerosis arising from low-grade inflammation over a protracted period of time, and our *in vivo* data confirm the importance of this receptor complex in both NLRP3 priming and atherosclerotic plaque formation. Notably, CD36 deficiency in *Apoe*$^{-/-}$ mice also causes a striking reduction in cholesterol crystal accumulation in plaques and serum IL-1 family cytokines (IL-1β, IL-1α, IL-18) concentrations, arguing that the CD36-dependent pathway for intracellular crystal generation identified *in vitro* is also active *in vivo*. The endocytosis of ligands by CD36, which leads to the nucleation of NLRP3 activators, can therefore be thought of as ‘Signal 0’ in models of inflammasome activation by sterile inflammatory stimuli, providing the common cellular event required for priming and activation of NLRP3 in metabolic diseases.

The incidence of atherosclerosis and T2D continues to increase and the development of new therapeutics for metabolic disease is crucial. The appreciation of the critical role of the NLRP3 inflammasome in both atherogenesis and T2D highlights the promise of this pathway for therapeutic targeting. Whilst many studies have described regulators of inflammasome activity at the level of complex assembly and caspase-1 activation[51], the identification of CD36 as a key upstream regulator of NLRP3 activation by endogenous danger ligands in atherosclerosis, AD and T2D provides a new target for the therapeutic intervention which does not compromise inflammasome activity required for host defense against pathogens. To our knowledge, this is the first such upstream regulator of NLRP3 described in sterile inflammation, with CD36 fulfilling a role analogous to the P2X7 receptor for ATP-mediated activation of NLRP3 (ref. 52). CD36 targeting for amelioration of NLRP3 activation may be particularly useful for atherosclerosis, where CD36 is essential for inflammasome priming and activation in macrophage foam cells, as well as the accumulation of cholesterol crystals in plaques. Supporting this, we find that targeting CD36 using antisense oligonucleotides reduces serum IL-1β concentrations in atherosclerotic mice, suggesting that such strategies may hold promise for reducing inflammasome activation in human disease.

METHODS

Mice & Cell Culture

Cd36$^{-/-}$, *Tlr4*$^{-/-}$, *Tlr6*$^{-/-}$, *Nlrp3*$^{-/-}$ and *Ice1*$^{-/-}$ mice were described[5, 31]. C57BL/6J mice were purchased from Jackson Laboratories. For peritoneal macrophage isolation, mice were injected intraperitoneally with 1mL 4% thioglycollate medium solution (Gibco) and peritoneal elicited cells isolated by washing the peritoneal cavity with 5 mL PBS 4 days post-injection. To separate macrophages, red blood cells were lysed and resulting cells seeded at 2×10^6 cell/mL in DMEM media (Gibco) containing 10% FBS. Macrophages were

allowed to adhere overnight and then media was changed to DMEM containing 2% FBS. Bone-marrow derived macrophages (BMDM) were isolated by flushing the bone marrow from femur and tibia of hind-legs from mice using DMEM containing 10% FBS supplemented with antibiotics as above. Cells were collected, centrifuged, lysed as above and resulting cells seeded at 1×10^6 cell/mL in DMEM containing 10% FBS and supplemented with conditioned media from L929 cells (15%) as described[53]. Cells were differentiated until day 5 after which they were harvested using 10 mM EDTA and plated at 1×10^6 cell/mL in DMEM containing 2% FBS and 7.5% L929 conditioned media. Immortalized macrophages stably transfected with a construct overexpresssing CFP-tagged murine ASC were described[11]. CHO cell lines stably transfected with plasmids overexpressing CD36 (CHOCD36) or empty vector control (CHO-eV) were described[30] and maintained in RPMI containing 10% FBS supplemented with antibiotics.

Mice & Atherosclerosis Studies

Apoe$^{-/-}$ and *Cd36*$^{-/-}$*Apoe*$^{-/-}$ mice were described[34]. *Tlr4*$^{-/-}$*Apoe*$^{-/-}$ and *Tlr6*$^{-/-}$*Apoe*$^{-/-}$ mice were generated by inter-crossing *Apoe*$^{-/-}$ and *Tlr4*$^{-/-}$ or *Tlr6*$^{-/-}$ mice on C57/BL6J background[31]. Double knock-out offspring were viable and born at a Mendelian ratio. All mice were housed in a pathogen-free environment in autoclaved filter-top cages with autoclaved water and kept on a 12-hour light/dark cycle. All experiments were approved by the New York University School of Medicine Institutional Animal Care and Use Committee. Beginning at 5-6 weeks of age, mice were fed a modified western diet (DYET#100244 containing 3 gm/kg cholesterol, Dyets Inc) for 12 weeks. At sacrifice, mice were anesthetized with isoflurane and exsanguinated by cardiac puncture. Hearts were perfused with PBS and the arterial system was perfusion-fixed with 10% formalin for lesion analysis or with RNA Later Soln. (Ambion) for RNA analysis. The heart and upper section of aorta was removed, cleaned of peripheral fat under a dissecting microscope and dissected directly under and parallel to the aortic leaflets. The upper section was embedded in OCT medium and snap-frozen immediately. For quantification of lesions in the aorta en face, the aorta was dissected so that it was free of all branching vessels, incised ventrally from the aortic root to the bifurcation of the iliac arteries and stored in PBS. Images of aortae were digitally captured and lesion area selected with IP Lab Spectrum software. Lesion area was calculated as a percentage of the total area of the whole aorta or defined regions of the aorta, including the aortic arch, thoracic, abdominal, and ileal areas (descending). Hearts embedded in OCT were sectioned through the aortic root (8 μm) and stained with hematoxylin and eosin for lesion quantification or used for immunofluoresence analysis. Serum was isolated from terminal bleeds at the time of sacrifice and used for determination of total cholesterol (Wako Cholesterol E kit) or stored frozen for analysis of cytokines. For experiments with CD36 antisense oligonucleotides, mice were injected with the CD36-specific ASO (CD36) or a non-targeting control ASO (Ctrl) provided by Isis Pharmaceuticals, at 50 mg/kg subcutaneously in endotoxin-free PBS (10 μL/g body weight). At 5 weeks of age mice were randomized into 2 groups (receiving Ctrl and CD36 ASO), bled for baseline measurements and received 2 injections spaced 2 days apart. One week post initial injection, mice were fed a western diet (DYET#100244) or 4 weeks, and continued to receive once weekly injections of ASO. Mice were bled at termination and serum cytokines were measured by ELISA. Both ASOs were 20-mer second generation MOE gapmers of the 5-10-5 design. Specifically, the phosphorothioate oligonucleotides contained 2'-0-(2-methoxyethyl)-modified ribonucleosides (2'-MOE) groups at positions 1 to 5 and 16 to 20 with 2'-deoxynucleosides at positions 6 to 15. The sequences of both ASOs were as follows: CD36 ASO, 5'-GAATGGATCTTTGTAACCCC-3' and Ctrl ASO, 5'-CCTTCCCTGAAGGTTCCTCC-3'. The Ctrl ASO does not hybridize to any known target and was used to control for any ASO class effects that could impact inflammasome activation

Reagents

Human LDL (BT-903) and acetylated LDL (BT-906) were obtained from Biomedical Technologies, Inc. For preparation of oxidized LDL (oxLDL), LDL was diluted in PBS to 250 μg/mL and dialysed overnight in 3L PBS at 4°C. Moderately oxidized LDL was prepared by dialysis against 5 μM $CuSO_4$ for 6h, and terminated by the addition of EDTA (200 nM) and butylated hydroxytlouene (500 nM). To obtain minimally modified LDL (mmLDL) and extensively oxidized LDL (ex-oxLDL) dialysis against against 5 μM $CuSO_4$ was terminated after 2h or 24h respectively. Cholesterol was obtained from Sigma-Aldrich and crystallized as described[7]. ATP and poly(dA:dT) [poly(dA-dT)•poly(dT-dA)] was from Sigma-Aldrich. poly(dA:dT) was delivered to the cytoplasm using transfection with Lipofectamine 2000 (Invitrogen). Amyloid-β (Aβ) and islet amyloid polypeptide (IAPP) peptides were obtained from California Peptides. Soluble β-amyloid (sAβ) was generated by resuspending human $Aβ_{1-42}$ peptide at 5 mg/mL in DMSO, distributed in aliquots and frozen immediately as described[30]. Non-amyloidogenic control reverse peptide (revAβ) was made soluble by similarly treating human $Aβ_{42-1}$ peptide. This method of preparation does not generate fibrillar Aβ as assessed by thioflavin-T fluorescence and electron microscopy. Soluble human IAPP (hIAPP) was resuspended in endotoxin-free water at 1 mg/mL as described[6]. Non-amyloidogenic control rat IAPP was prepared similarly. All reagents were sterile and endotoxin-free, as confirmed by Limulus amebocyte lysate testing using PYROGENT kit (Lonza). Ultrapure LPS (Alexis) was used at 200 ng/mL for 6 h for priming. In some experiments, following 6 h priming, media was changed to DMEM containing 2% FBS and cells were pretreated with the following inhibitors for 1 h before stimulation with NLRP3 activators; cytochalasin-D, bafilomycin-A1, Congo red (all from Sigma-Aldrich), or Lalistat (kind gift of F. Maxfield, Weill Cornell, NY). The broad spectrum caspase inhibitor ZVAD-fmk (benzyloxycarbonyl-Val-Ala-Asp-fluoromethylketone), the caspase-1 specific inhibitor z-YVAD-fmk (benzyloxycarbonyl-Tyr-Val-Ala-Asp-fluoromethylketone) and z-FA-fmk (benzyloxycarbonyl-Phe-Ala-fluoromethylketone), an irreversible inhibitor of cysteine proteases that do not require a P1 Asp residue, such as cathepsin B, L, and S, were from Santa Cruz Biotechnology Inc. In some experiments cells were pretreated with BAY 11-7082 (Calbiochem) or diphenyliodonium chloride (DPI – Sigma-Aldrich) 1 h prior to priming.

Molecular biology

RNA was isolated from cells/tissues using TRIzol reagent (Invitrogen/now Ambion) according to the manufacturers protocol. 1 μg RNA was reverse-transcribed to generate cDNA using the iScript cDNA Synthesis Kit (Bio-Rad). Gene expression was measured by real-time quantitative RT-PCR (qRT-PCR) using SYBR Green for quantification (KAPA SYBR FAST Universal qPCR Kit – KAPA Biosystems), on an Eppendorf realplex[4] Mastercycler platform. Primers sequences are listed below and each primer pair was tested to find optimal primer concentration prior to use, commonly between 100-200 nM. Ct values for each gene were normalized to housekeeping genes *Gapdh* or *Hprt* and relative expression calculated using the ΔΔCt method. Murine primer sequences used were: *Gapdh*; Fwd 5'-AGGTCGGTGTGAACGGATTTG-3', Rev 5'-TGTAGACCATGTAGTTGAGGTCA-3', *Hprt*; Fwd 5'-TCAGTCAACGGGGGACATAAA-3', Rev 5'-GGGGCTGTACTGCTTAACCAG-3', *Il1b*; Fwd 5'-TGTGAATGCCACCTTTTGACA-3', Rev 5'-GGTCAAAGGTTTGGAAGCAG-3', *Il1a*; Fwd 5'-GCACCTTACACCTACCAGAGT-3', Rev 5'-AAACTTCTGCCTGACGAGCTT-3', *Il18*; Fwd 5'-GACTCTTGCGTCAACTTCAAGG-3', Rev 5'-CAGGCTGTCTTTTGTCAACGA-3', *Nlrp3*; Fwd 5'-ATTACCCGCCCGAGAAAGG-3', Rev 5'-TCGCAGCAAAGATCCACACAG-3', *Nlrc4*; Fwd 5'-TTGAAGGCGAGTCTGGCAAAG-3', Rev 5'-GGCGCTTCTCAGGTGGATG-3', and *Cd36*; Fwd 5'-ATGGGCTGTGATCGGAACTG-5', Rev 5'-

GTCTTCCCAATAAGCATGTCTCC-3';. Silencing of CD36 *in vitro* was assessed by transfection of immortalized macrophages with 10 ng ASO per well in 12 well plates using Lipofectamine RNAiMax (Invitrogen).

Serum array and ELISA

Mouse serum was used for multiplex analysis of cytokines using Quantibody Mouse Inflammation Array 1 (QAM-INF-1 – Raybiotech Inc.) according to the manufacturers instructions. Serum IL-18 ELISA was performed using Mouse IL-18 ELISA Kit (MBL - #7625). ELISA analysis of supernatants was performed using specific DuoSet ELISA kits from R&D Systems - IL-1β (DY401) and IL-1α (DY400).

Microscopy

For analysis of speck formation using ASC-CFP transfected macrophages, cells were seeded in 8-well Lab-Tek chamber slides (Thermo Scientific) and following the experiment fixed in 4% paraformaldehye (IC Fixation Buffer, 1x concentrate - Invitrogen), washed with PBS and stained using Alexa Fluor 594-coupled cholera toxin subunit B (AF594-CTB - Invitrogen) at 2 μg/mL and counterstained with 4',6-Diamidino-2-Phenylindole (DAPI - Sigma) at 0.5 μg/mL prior to mounting with Fluorescent Mounting Medium (Dako). Cells were visualized using Confocal Microscopy (Zeiss 600 System). Images taken at 63X were merged using ImageJ. For quantification of speck formation, images were taken using epifluoresence microscopy at 20X. For analysis of crystal formation alongside lysosomal markers live cell imaging was performed. Briefly, cells were seeded in 35 mm petri dishes on 0.16 mm coverglasses and allowed to adhere overnight. Cells were then pre-treated with Alexa Fluor 647-coupled Dextran (10 kDa MW - Invitrogen) at 50 μg/mL or Lysotracker Red DND-99 at 100 nM for 1 h prior to treatment with inflammasome activators. Combined confocal reflection microscopy was performed at various time points using a Leica SP2 AOBS confocal laser-scanning microscope as described[13]. For analysis of amyloid formation cells were seeded in 8-well Lab-Tek chamber slides as above and following the experiments fixed in 10% paraformaldehyde, washed with PBS, stained using AF594-CTB as before, washed with PBS, permeabilized using 0.1 % Triton X-100 for 20 min followed by staining with 0.01 % thioflavin-S. After staining cells were washed five times with 70 % EtOH followed by 2 washes with PBS, stained with DAPI and mounted as above. Cells were imaged using a Nikon Ti (Eclipse) inverted microscope with Ultraview Spinning Disc (CSU-X1) confocal scanner (Perkin Elmer). Images were captured with an Orca-ERCamera using Volocity (Perkin Elmer). Post acquisition analysis such as contrast adjustment, deconvolution through iterative restoration and 3D reconstruction were performed using Volocity software.

Immunofluoresence staining

Slides containing 8 sections covering the aortic root were fixed in acetone, blocked using 10 % serum (specific to species secondary antibodies were raised in) in PBS and stained with antibodies for CD68 (rat anti-mouse IgG, Serotec) as described before or IL1β (goat anti-mouse IgG, AF-401-A, R&D Systems) at 1 μg/mL at 4°C overnight. Slides were washed and incubated with Alexa Fluor-coupled secondary antibodies: AF-568 goat anti-rat IgG for CD68 stains, AF-568 rabbit anti-goat IgG for IL-1β staining, at 2 μg/mL for 2 h at 21 °C. Sections were then incubated with fluorescent peptide-based probes for active caspase-1 (FAM-YVAD-fmk – FLICA Caspase 1 Kit #98 – ImmunoChemistry Technologies) used at 3X, 2h at 21 °C. Slides were then washed and counterstained with DAPI before mounting as above. Aortic root plaques were visualized using epifluoresence microscopy. For quantification of caspase-1 activity and IL-1β staining, the area positive for staining in plaques was expressed as a percentage of total area using Image J software. For analysis of plaque crystal content, tissue sections were fixed with 4 % paraformaldehyde to preserve

crystalline material, nuclei were stained with Hoechst 33342 (Immunochemistry) and combined confocal reflection microscopy was performed using a Leica TCS SP5 II AOBS confocal laser-scanning microscope as described[13]. Plaque crystal content was quantified using Volocity Quantitation (Perkin Elmer) and is expressed as a percentage of total plaque area.

Flow Cytometry

For evaluation of lysosomal damage, cells were incubated with Lysotracker Red DND-99 (1 μM) for 1 h prior to stimulation with inflammasome activators. Lysosomal damage was defined as loss of Lysotracker fluorescence, as assessed by flow cytometry. For evaluation of binding of soluble peptides, a fluorescently tagged human IAPP peptide which contains a fluorescent dye conjugate on the N terminus (FAM-huIAPP) or Hilyte-Fluor 488 conjugated human $A\beta_{1–42}$ (488-Aβ) were obtained from AnaSpec Inc., Freemont, CA and made soluble as described above. Binding to CHO cells was determined following 2 h incubations using flow cytometry to measure associated fluorescence as described[54]. Briefly, extracellular fluorescence was quenched with 0.2% trypan blue shortly before analysis and binding was calculated as the difference between total cell-associated fluorescence and intracellular fluorescence. All flow cytometry measurements were carried out using an Accuri C6 Flow Cytometer (BD Biosciences).

Statistical analysis

Statistical significance was assessed by a one way analysis of variance for multiple comparisons or an unpaired, two-tailed Student's t-test for single comparison. A P value of less than 0.05 was considered significant.

Supplementary Material

Refer to Web version on PubMed Central for supplementary material.

Acknowledgments

This work was supported by the National Institutes of Health (R01HL117334 and R01AG032349 to KJM; U24 AI082660 to LMS and KJM; R01 AI079198 to LMS; 5R01HL093262-02 and 1R01HL112661-01 to EL; AI083713 to KAF and EL) and the American Heart Association (11POST7400075 to FJS). We would like to thank F.gg Maxfield (Weill Cornell Medical College, NY) for providing the Lalistat inhibitor.

REFERENCES

1. Abela GS. Cholesterol crystals piercing the arterial plaque and intima trigger local and systemic inflammation. J. Clin. Lipidol. 2010; 4:156–164. [PubMed: 21122648]
2. Meyer-Luehmann M, et al. Rapid appearance and local toxicity of amyloid-beta plaques in a mouse model of Alzheimer's disease. Nature. 2008; 451:720–724. [PubMed: 18256671]
3. Westermark GT, Westermark P, Berne C, Korsgren O. Nordic Network for Clinical Islet T. Widespread amyloid deposition in transplanted human pancreatic islets. N. Engl. J. Med. 2008; 359:977–979. [PubMed: 18753660]
4. Duewell P, et al. NLRP3 inflammasomes are required for atherogenesis and activated by cholesterol crystals. Nature. 2010; 464:1357–1361. [PubMed: 20428172]
5. Halle A, et al. The NALP3 inflammasome is involved in the innate immune response to amyloid-beta. Nat. Immunol. 2008; 9:857–865. [PubMed: 18604209]
6. Masters SL, et al. Activation of the NLRP3 inflammasome by islet amyloid polypeptide provides a mechanism for enhanced IL-1beta in type 2 diabetes. Nat. Immunol. 2010; 11:897–904. [PubMed: 20835230]

7. Rajamaki K, et al. Cholesterol crystals activate the NLRP3 inflammasome in human macrophages: a novel link between cholesterol metabolism and inflammation. PLoS One. 2010; 5:e11765. [PubMed: 20668705]
8. Kuida K, et al. Altered cytokine export and apoptosis in mice deficient in interleukin-1 beta converting enzyme. Science. 1995; 267:2000–2003. [PubMed: 7535475]
9. Keller M, Ruegg A, Werner S, Beer HD. Active caspase-1 is a regulator of unconventional protein secretion. Cell. 2008; 132:818–831. [PubMed: 18329368]
10. Bauernfeind F, et al. Reactive oxygen species inhibitors block priming, but not activation, of the NLRP3 inflammasome. J Immunol. 2011; 187:613–617. [PubMed: 21677136]
11. Bauernfeind FG, et al. NF-kappaB activating pattern recognition and cytokine receptors license NLRP3 inflammasome activation by regulating NLRP3 expression. J Immunol. 2009; 183:787–791. [PubMed: 19570822]
12. Embry CA, Franchi L, Nunez G, Mitchell TC. Mechanism of impaired NLRP3 inflammasome priming by monophosphoryl lipid A. Sci Signal. 2011; 4:ra28. [PubMed: 21540455]
13. Hornung V, et al. Silica crystals and aluminum salts activate the NALP3 inflammasome through phagosomal destabilization. Nat. Immunol. 2008; 9:847–856. [PubMed: 18604214]
14. Zhou R, Yazdi AS, Menu P, Tschopp J. A role for mitochondria in NLRP3 inflammasome activation. Nature. 2011; 469:221–225. [PubMed: 21124315]
15. Williams KJ, Tabas I. The response-to-retention hypothesis of early atherogenesis. Arterioscler. Thromb. Vasc. Biol. 1995; 15:551–561. [PubMed: 7749869]
16. Lim RS, et al. Identification of cholesterol crystals in plaques of atherosclerotic mice using hyperspectral CARS imaging. J. Lipid Res. 2011; 52:2177–2186. [PubMed: 21949051]
17. Haass C, et al. Amyloid beta-peptide is produced by cultured cells during normal metabolism. Nature. 1992; 359:322–325. [PubMed: 1383826]
18. Kirschner DA, et al. Synthetic peptide homologous to beta protein from Alzheimer disease forms amyloid-like fibrils in vitro. Proc. Natl. Acad. Sci. USA 84. 1987:6953–6957.
19. Seubert P, et al. Isolation and quantification of soluble Alzheimer's beta-peptide from biological fluids. Nature. 1992; 359:325–327. [PubMed: 1406936]
20. Clark A, et al. Islet amyloid formed from diabetes-associated peptide may be pathogenic in type-2 diabetes. Lancet. 1987; 2:231–234. [PubMed: 2441214]
21. Cooper GJ, et al. Purification and characterization of a peptide from amyloid-rich pancreases of type 2 diabetic patients. Proc. Natl. Acad. Sci. USA. 1987; 84:8628–8632. [PubMed: 3317417]
22. Westermark P, et al. Amyloid fibrils in human insulinoma and islets of Langerhans of the diabetic cat are derived from a neuropeptide-like protein also present in normal islet cells. Proc. Natl. Acad. Sci. USA. 1987; 84:3881–3885. [PubMed: 3035556]
23. Badman MK, Pryce RA, Charge SB, Morris JF, Clark A. Fibrillar islet amyloid polypeptide (amylin) is internalised by macrophages but resists proteolytic degradation. Cell Tissue Res. 1998; 291:285–294. [PubMed: 9426315]
24. de Koning EJ, et al. Macrophages and pancreatic islet amyloidosis. Amyloid. 1998; 5:247–254. [PubMed: 10036582]
25. Haass C, Koo EH, Mellon A, Hung AY, Selkoe DJ. Targeting of cell-surface beta-amyloid precursor protein to lysosomes: alternative processing into amyloid-bearing fragments. Nature. 1992; 357:500–503. [PubMed: 1608449]
26. Hartmann T, et al. Distinct sites of intracellular production for Alzheimer's disease A beta40/42 amyloid peptides. Nat. Med. 1997; 3:1016–1020. [PubMed: 9288729]
27. Silverstein RL, Febbraio M. CD36, a scavenger receptor involved in immunity, metabolism, angiogenesis, and behavior. Sci. Signal. 2009; 2:re3. [PubMed: 19471024]
28. Kunjathoor VV, et al. Scavenger receptors class A-I/II and CD36 are the principal receptors responsible for the uptake of modified low density lipoprotein leading to lipid loading in macrophages. J. Biol. Chem. 2002; 277:49982–49988. [PubMed: 12376530]
29. Moore KJ, et al. A CD36-initiated signaling cascade mediates inflammatory effects of beta-amyloid. J. Biol. Chem. 2002; 277:47373–47379. [PubMed: 12239221]

30. Wilkinson K, Boyd JD, Glicksman M, Moore KJ, El Khoury J. A high content drug screen identifies ursolic acid as an inhibitor of amyloid beta protein interactions with its receptor CD36. J. Biol. Chem. 2011; 286:34914–34922. [PubMed: 21835916]
31. Stewart CR, et al. CD36 ligands promote sterile inflammation through assembly of a Toll-like receptor 4 and 6 heterodimer. Nat. Immunol. 2010; 11:155–161. [PubMed: 20037584]
32. El Khoury JB, et al. CD36 mediates the innate host response to beta-amyloid. J. Exp. Med. 2003; 197:1657–1666. [PubMed: 12796468]
33. Febbraio M, et al. Targeted disruption of the class B scavenger receptor CD36 protects against atherosclerotic lesion development in mice. J. Clin. Invest. 2000; 105:1049–1056. [PubMed: 10772649]
34. Moore KJ, et al. Loss of receptor-mediated lipid uptake via scavenger receptor A or CD36 pathways does not ameliorate atherosclerosis in hyperlipidemic mice. J. Clin. Invest. 2005; 115:2192–2201. [PubMed: 16075060]
35. Goudriaan JR, et al. CD36 deficiency increases insulin sensitivity in muscle, but induces insulin resistance in the liver in mice. J. Lipid. Res. 2003; 44:2270–2277. [PubMed: 12923231]
36. Hajri T, Han XX, Bonen A, Abumrad NA. Defective fatty acid uptake modulates insulin responsiveness and metabolic responses to diet in CD36-null mice. J. Clin. Invest. 2002; 109:1381–1389. [PubMed: 12021254]
37. Kennedy DJ, et al. A CD36-dependent pathway enhances macrophage and adipose tissue inflammation and impairs insulin signalling. Cardiovasc. Res. 2011; 89:604–613. [PubMed: 21088116]
38. Binder CJ, et al. Pneumococcal vaccination decreases atherosclerotic lesion formation: molecular mimicry between Streptococcus pneumoniae and oxidized LDL. Nat. Med. 2003; 9:736–743. [PubMed: 12740573]
39. Schmitz G, Grandl M. Endolysosomal phospholipidosis and cytosolic lipid droplet storage and release in macrophages. Biochim. Biophys. Acta. 2009; 1791:524–539. [PubMed: 19146988]
40. Rosenbaum AI, et al. Chemical screen to reduce sterol accumulation in Niemann-Pick C disease cells identifies novel lysosomal acid lipase inhibitors. Biochim. Biophys. Acta. 2009; 1791:1155–1165. [PubMed: 19699313]
41. Heneka MT, et al. NLRP3 is activated in Alzheimer's disease and contributes to pathology in APP/PS1 mice. Nature. 2013; 493:674–678. [PubMed: 23254930]
42. Friedrich RP, et al. Mechanism of amyloid plaque formation suggests an intracellular basis of Abeta pathogenicity. Proc. Natl. Acad. Sci. USA. 2010; 107:1942–1947. [PubMed: 20133839]
43. Walsh DM, Tseng BP, Rydel RE, Podlisny MB, Selkoe DJ. The oligomerization of amyloid beta-protein begins intracellularly in cells derived from human brain. Biochemistry. 2000; 39:10831–10839. [PubMed: 10978169]
44. Miao EA, et al. Caspase-1-induced pyroptosis is an innate immune effector mechanism against intracellular bacteria. Nat. Immunol. 2010; 11:1136–1142. [PubMed: 21057511]
45. Kamari Y, et al. Reduced atherosclerosis and inflammatory cytokines in apolipoprotein-E-deficient mice lacking bone marrow-derived interleukin-1alpha. Biochem. Biophys. Res. Commun. 2011; 405:197–203. [PubMed: 21219852]
46. Kuchibhotla S, et al. Absence of CD36 protects against atherosclerosis in ApoE knock-out mice with no additional protection provided by absence of scavenger receptor A I/II. Cardiovasc. Res. 2008; 78:185–196. [PubMed: 18065445]
47. Chen CJ, et al. Identification of a key pathway required for the sterile inflammatory response triggered by dying cells. Nat. Med. 2007; 13:851–856. [PubMed: 17572686]
48. Rasmussen LT, Seljelid R. The modulatory effect of lipoproteins on the release of interleukin 1 by human peritoneal macrophages stimulated with beta-1,3-D-polyglucose derivatives. Scand. J. Immunol. 1989; 29:477–484. [PubMed: 2497512]
49. Thomas CE, Jackson RL, Ohlweiler DF, Ku G. Multiple lipid oxidation products in low density lipoproteins induce interleukin-1 beta release from human blood mononuclear cells. J. Lipid Res. 1994; 35:417–427. [PubMed: 8014577]
50. Moyer CF, Sajuthi D, Tulli H, Williams JK. Synthesis of IL-1 alpha and IL-1 beta by arterial cells in atherosclerosis. Am. J. Pathol. 1991; 138:951–960. [PubMed: 2012178]

51. Guarda G, So A. Regulation of inflammasome activity. Immunology. 2010; 130:329–336. [PubMed: 20465574]

52. Mariathasan S, et al. Cryopyrin activates the inflammasome in response to toxins and ATP. Nature. 2006; 2006; 440:228–232. [PubMed: 16407890]

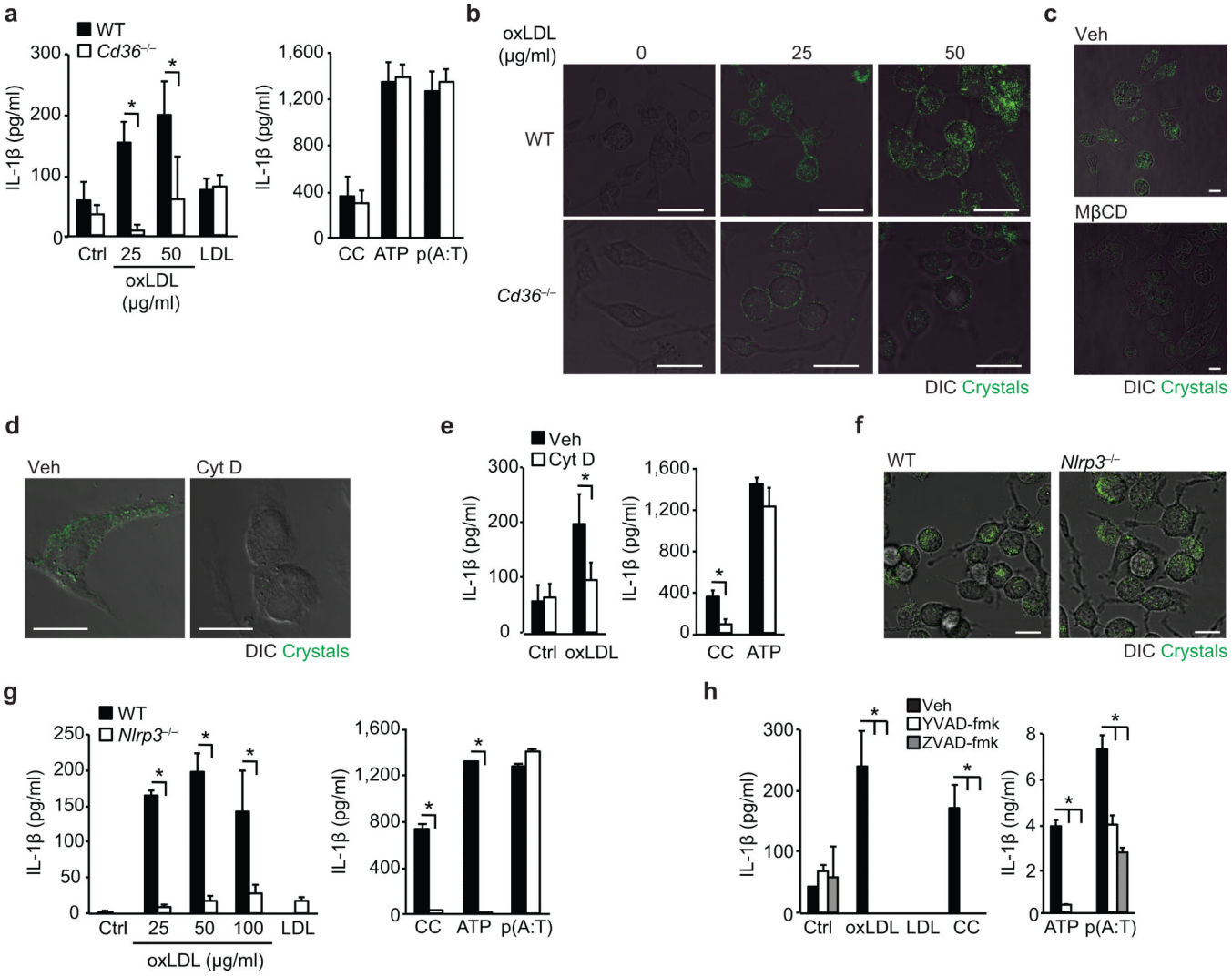

Figure 1. CD36-mediated uptake of oxLDL generates intracellular crystals and activates the NLRP3 inflammasome

(a) IL-1β ELISA of supernatants from LPS-primed wild-type (WT) or CD36-deficient (*Cd36*$^{-/-}$) BMDM incubated for 24 h with PBS vehicle (Ctrl), oxLDL or unmodified LDL (left panel) alongside the following inflammasome activators (right panel), cholesterol crystals (CC, 1 mg/mL), ATP (5 μM, 1 h) and poly(dA:dT) [p(A:T), 100 ng/well, 6 h]. **(b)** Confocal reflection microscopy of WT or *Cd36*$^{-/-}$ peritoneal macrophages treated for 24 h with oxLDL as indicated. **(c)** Confocal reflection microscopy of peritoneal macrophages treated with oxLDL (50 μg/mL, 24 h) and subsequently treated with methyl-β-cyclodextrin (MβCD, 10 μM, 1 h) or vehicle (Veh). **(d)** Confocal reflection microscopy of oxLDL-treated BMDM (50 μg/mL, 24 h) following pre-treatment with cytochalasin D (Cyt D (1 μM, 1 h) or vehicle control (Veh). **(e)** IL-1β ELISA of supernatants from LPS-primed BMDM treated for 24 h with PBS vehicle (Ctrl), oxLDL (50 μg/mL) or cholesterol crystals and ATP as before. **(f)** Confocal reflection microscopy of WT or NLRP3-deficient (*Nlrp3*$^{-/-}$) BMDM treated with oxLDL (50 μg/mL, 24 h). **(g)** IL-1β ELISA of supernatants from LPS-primed WT or *Nlrp3*$^{-/-}$ BMDM treated as in a). **(h)** IL-1β ELISA of supernatants from LPS-primed BMDM treated with the indicated inflammasome activators following 1 h pre-treatment with ZVAD-fmk (pan-caspase inhibitor, 20 μM) or YVAD-fmk (caspase-1

inhibitor, 20 μM). Data in a, e, g and h are mean ± s.d. of triplicate samples within a single experiment and are representative of three independent experiments. Images in b, c,d and f are representative of 3 independent experiments. Scale bar = 10 μm. *P<0.05.

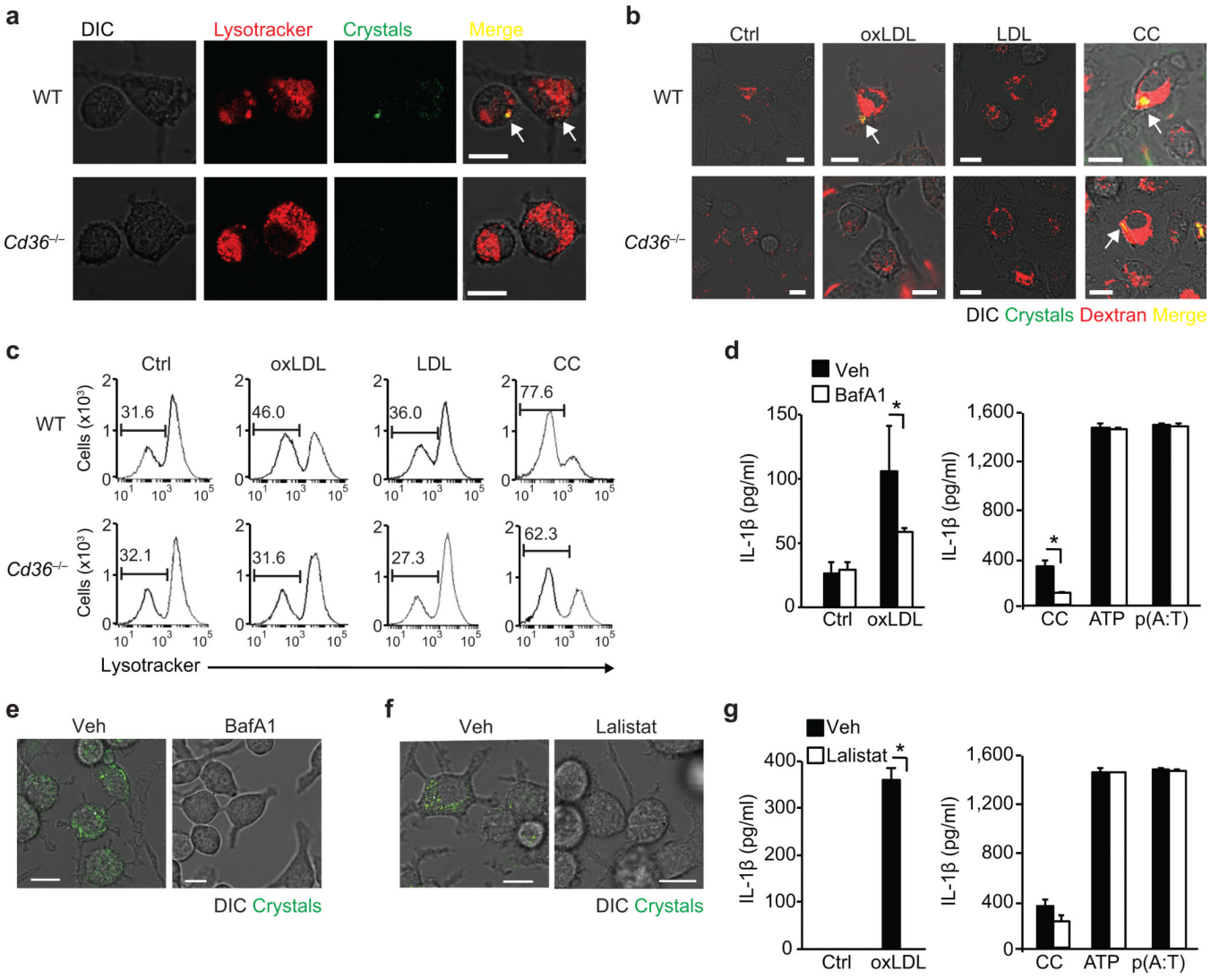

Figure 2. CD36-mediated cholesterol crystal formation and NLRP3 activation occurs via a lysosomal pathway

(a) Combined confocal reflection microscopy of wild-type (WT) or CD36-deficient (*Cd36*$^{-/-}$) BMDM incubated for 8 h with oxLDL (50 μg/mL) alongside Lysotracker-Red. **(b)** Combined confocal reflection microscopy of WT or *Cd36*$^{-/-}$ BMDM incubated for 24 h with PBS vehicle (Ctrl), oxLDL (50 μg/mL), unmodified LDL (50 μg/mL) or cholesterol crystals (CC, 1 mg/mL) alongside fluorescent Dextran-Red. **(c)** Flow cytometry measurements of Lysotracker Red-fluoresence in WT or *Cd36*$^{-/-}$ BMDM treated as in (b). **(d,g)** IL-β ELISA of supernatants from LPS-primed BMDM incubated the indicated inflammasome activators following pre-treatment with 500 nM bafilomycin A1 (BafA1) (d) or 20 nM Lalistat (g). **(e,f)** Confocal reflection microscopy of oxLDL-loaded BMDM (50 μg/mL, 24 h) following pre-treatment with BafA1 or Lalistat (as in d and g). Data in d and g are mean ± s.d. of triplicate samples within a single experiment and are representative of three independent experiments. Images in a-c, e and f are representative of three independent experiments. Scale bar = 10 μm. *P<0.05.

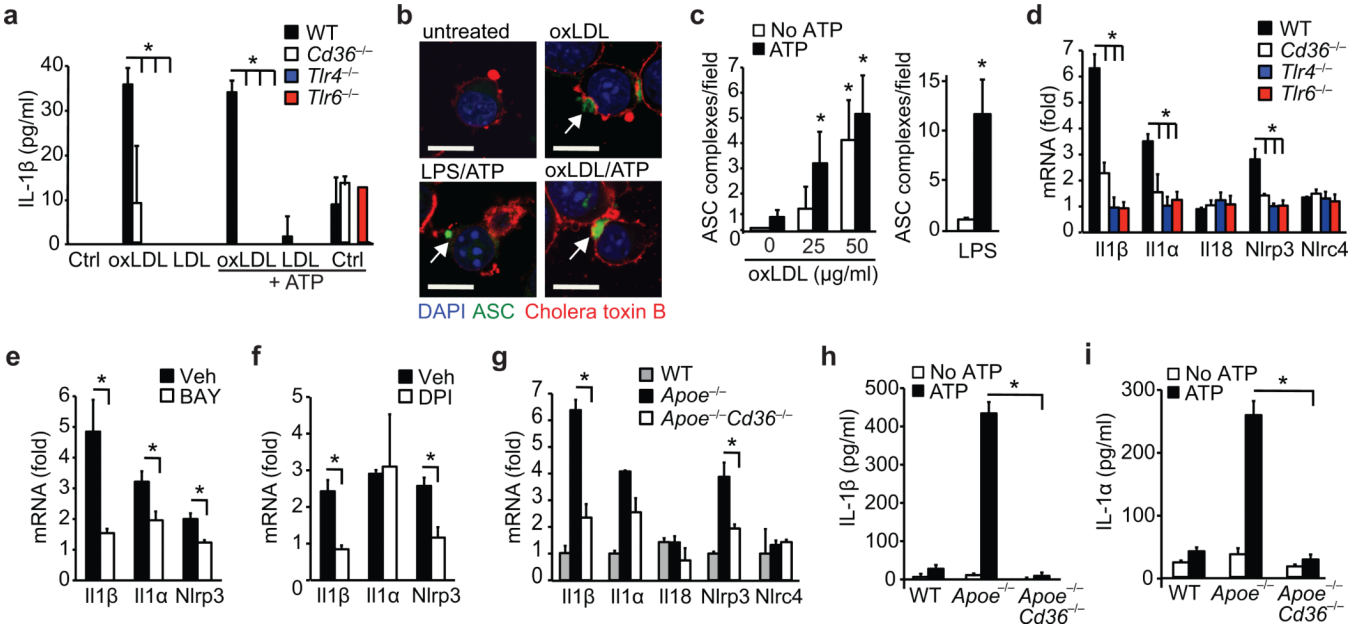

Figure 3. CD36 regulates priming of the NLRP3 inflammasome by oxLDL through TLR4-TLR6

(a) IL-1β ELISA of supernatants from wild-type (WT), CD36-deficient (*Cd36*$^{-/-}$), TLR4-deficient (*Tlr4*$^{-/-}$) or TLR6-deficient (*Tlr6*$^{-/-}$) peritoneal macrophages primed with oxLDL, unmodified LDL (50 μg/mL, 18 h) or PBS vehicle (Ctrl) and subsequently treated with ATP (5 μM, 1 h). **(b)** Confocal microscopy of ASC-CFP expressing immortalized macrophages treated as indicated. **(c)** Quantification of ASC-oligomerization (speck formation) per 20x field for the indicated treatments. **(d-f)** Relative mRNA expression of the indicated gene in oxLDL-treated WT, *Cd36*$^{-/-}$, *Tlr4*$^{-/-}$ or *Tlr6*$^{-/-}$ peritoneal macrophages (d) or from WT peritoneal macrophages following pre-treatment with BAY 11-7083 (BAY, an NF-κB inhibitor, 10 μM,) (e) or diphenylene iodonium (DPI, an NAPDH oxidase inhibitor, 1 μM) (f), measured by qRT-PCR. **(g)** Relative mRNA expression in *in-vivo* formed foam cell macrophages from mice of the indicated genotype fed a western diet and expressed relative to macrophages from chow-fed mice. **(h-i)** IL-1β (h) or IL-1α (i) production from *in-vivo* formed foam cells from mice of the indicated genotype treated *ex-vivo* with ATP (5 μM, 1 h). Data in a, h-i are mean ± s.d. of triplicate samples within a single experiment and are representative of three independent experiments. Data in c-f and g is mean ± s.e.m. of three independent experiments. Images in b are representative of three independent experiments. Scale bar =10 μm. *P<0.05.

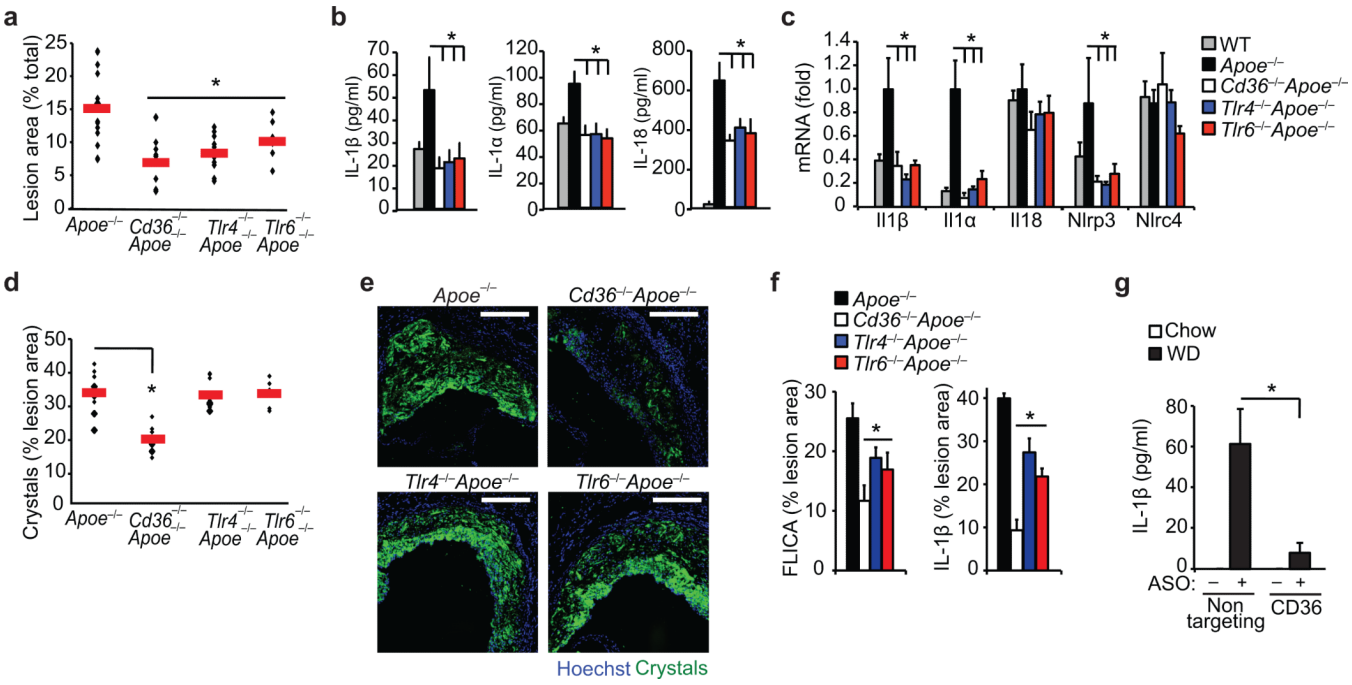

Figure 4. Inflammasome activity is impaired in atherogenic mice deficient in CD36 and its signaling partners TLR4 and TLR6

Mice of the indicated genotype (*Apoe*$^{-/-}$, *Cd36*$^{-/-}$*Apoe*$^{-/-}$, *Tlr4*$^{-/-}$ *Apoe*$^{-/-}$, *Tlr6*$^{-/-}$*Apoe*$^{-/-}$, or control C57/BL6 *Apoe*$^{+/+}$) were fed a western diet for 12 weeks, and atherosclerosis and inflammasome activity was assessed. **(a)** Lesion area in the aorta *en face* measured as a % of total aortic area. **(b)** Serum cytokine concentrations measured by Raybiotech Protein Array (IL1β, IL1α) or ELISA (IL18). **(c)** qRT-PCR analysis of aortic mRNA. **(d-e)** Plaque crystal content measured in serial sections throughout aortic root by combined confocal reflection microscopy illustrated in (e) and quantified in (d). **(f)** Plaque caspase-1 activity measured in serial sections throughout aortic root using FAM-YVAD-fmk FLICA probe fluorescence (left) or anti-IL-1β immunofluorescent staining (right) (n=8 sections/mouse) and expressed as % of total plaque area. **(g)** Serum IL-1β concentrations from *Apoe*$^{-/-}$ mice before (chow) or after western diet (WD) feeding for 4 wk during which mice were treated with a non-targeting or CD36 antisense oligonucleotide (ASO). Data is presented for n=15 mice (*Apoe*$^{-/-}$), n=10 mice/group (*Cd36*$^{-/-}$*Apoe*$^{-/-}$ and *Tlr4*$^{-/-}$*Apoe*$^{-/-}$) and n=7 mice (*Tlr6*$^{-/-}$*Apoe*$^{-/-}$) (a,d). Horizontal bars indicate the mean and symbols indicate individual mice. All other data is mean ± s.e.m. for n=4 mice/group (b-c), n=6 mice/group (f) and n=5 mice/group (g). Scale bar = 200 μm. *P<0.05.

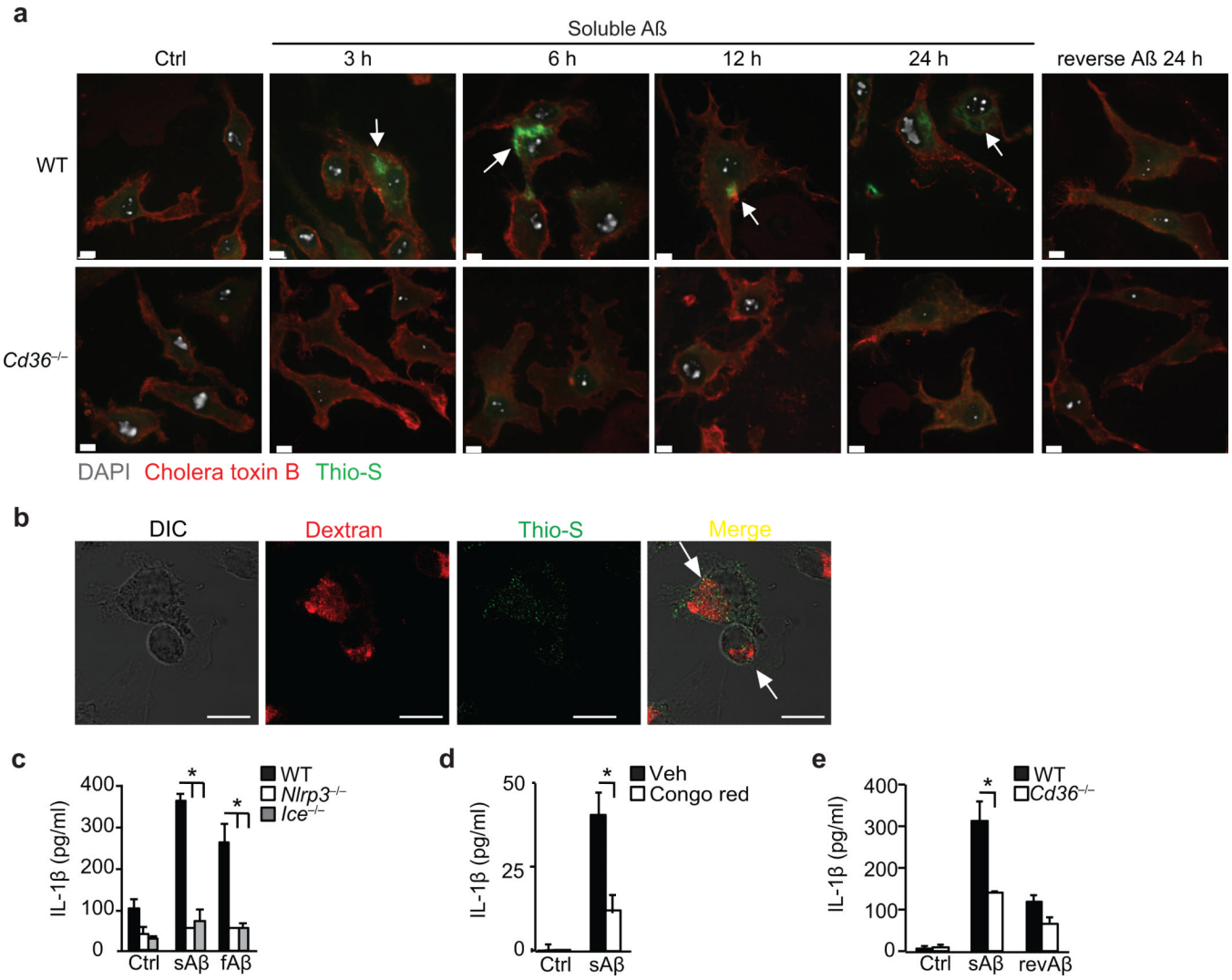

Figure 5. CD36 uptake of soluble Aβ induces intracellular NLRP3-activating amyloid formation

(a) Confocal microscopy of wild-type (WT) or CD36-deficient (*Cd36*$^{-/-}$) BMDM incubated with 10 μM soluble Aβ for the indicated times or control reverse peptide (reverse Aβ) for 24 h. After incubation cells were fixed and stained with Alexa-568 conjugated cholera toxin B and thioflavin-S (Thio-S) to visualize intracellular amyloid. **(b)** Confocal microscopy of BMDM incubated for 6 h with soluble Aβ (10 μM) and fluorescent Dextran as a lysosomal marker, then fixed and stained with thioflavin-S to visualize intracellular amyloid. **(c)** IL-1β ELISA of supernatants from LPS primed WT, NLRP3-deficient (*Nlrp3*$^{-/-}$) or Caspase-1 deficient (*Ice*$^{-/-}$) BMDM treated for 24h with DMSO-vehicle (Ctrl), soluble Aβ (sAβ, 10 μM) or fibrillar β-amyloid (fAβ, 1 μM). **(d)** IL-β ELISA of supernatants from LPS-primed BMDM pre-treated with Congo red (200 μM) for 1 h and incubated for 24h with DMSO vehicle (Ctrl) or sAβ (10 μM). **(e)** IL-1β ELISA of supernatants from LPS primed WT or *Cd36*$^{-/-}$ BMDM treated for 24 h with DMSO-vehicle (Ctrl), sAβ (10 μM) or reverse peptide (revAβ, 10 μM). Data in c-e are mean ± s.d. of triplicate samples within a single experiment and are representative of three independent experiments. Images in a-b are representative of three independent experiments. Scale bar = 10 μm. *P<0.05.

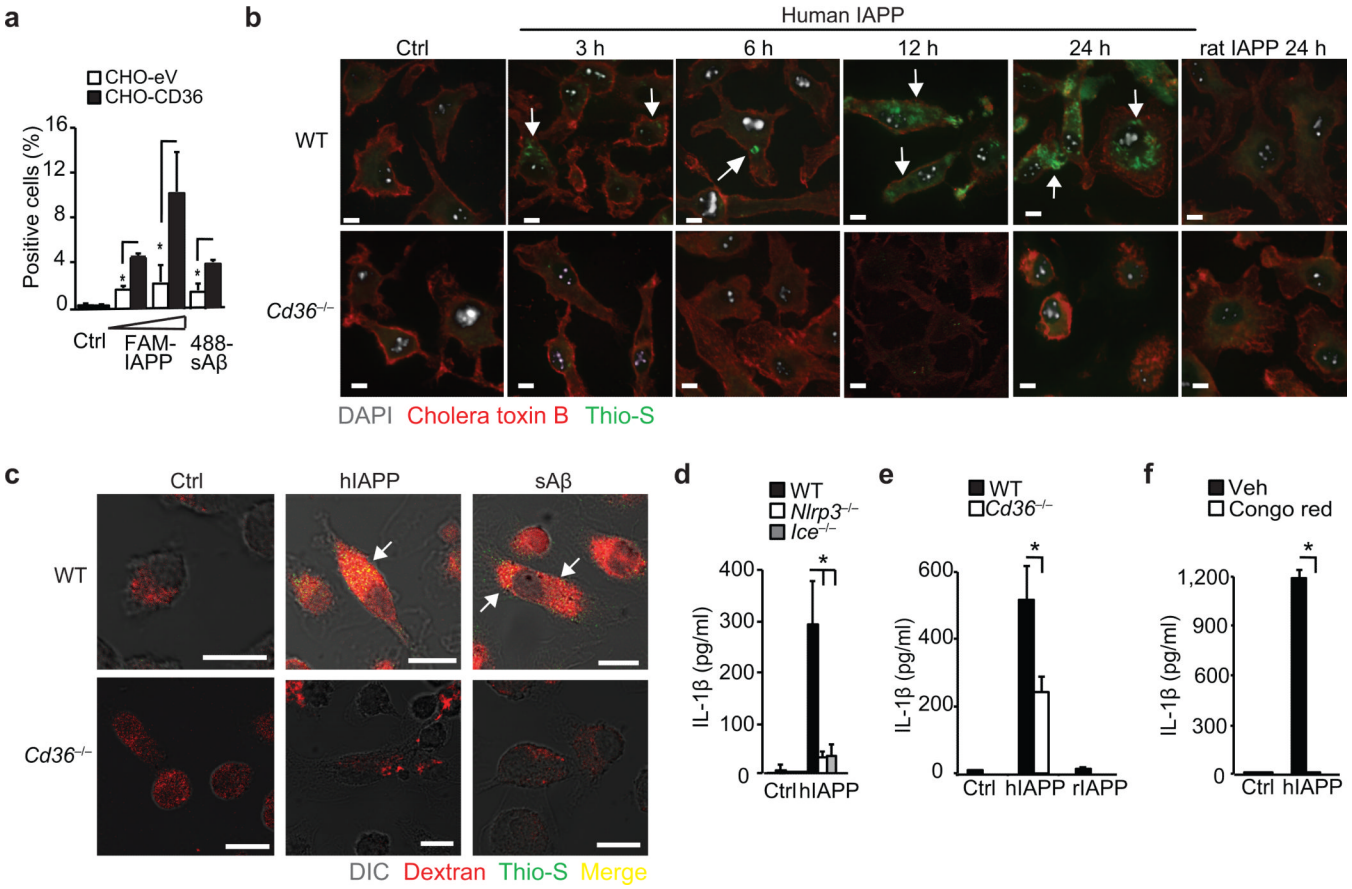

Figure 6. CD36 regulates NLRP3 activation by IAPP

(a) Binding of FAM-conjugated human IAPP, (FAM-IAPP; 5-10 μM) and HiLyte-488-conjugated soluble Aβ (488-sAβ) to control (CHO-eV) or CD36-expressing CHO (CHO-CD36) cells. **(b)** Confocal microscopy of WT or *Cd36*$^{-/-}$ BMDM incubated with 10 μM soluble human IAPP for the indicated times or control rat IAPP for 24 h. Cells were fixed and stained with Alexa-568 conjugated cholera toxin B and thioflavin-S (Thio-S) to visualize intracellular amyloid. **(c)** Confocal microscopy of WT or *Cd36*$^{-/-}$ BMDM incubated with human IAPP (hIAPP) or soluble Aβ (sAβ, 10 μM, 24 h) and fluorescent Dextran-Red, then fixed and stained with thioflavin-S. Arrows indicate thioflavin-S-reactive amyloid. **(d)** IL-1β ELISA of supernatants from LPS primed WT, NLRP3-deficient (*Nlrp3*$^{-/-}$) or Caspase-1 deficient (*Ice*$^{-/-}$) BMDM treated for 6 h with vehicle (Ctrl) or huIAPP (10 μM). **(e)** IL-1β ELISA of supernatants from LPS primed WT or *Cd36*$^{-/-}$ BMDM treated for 6h with vehicle (Ctrl), hIAPP (10 μM) or control rat IAPP (rIAPP, 10 μM). **(f)** IL-β ELISA of supernatants from LPS-primed BMDM pre-treated with Congo Red (200 μM, 1 h) and incubated for 6 h with vehicle (Ctrl) or hIAPP (10 μM). Data in a, d-f are mean ± s.d. of triplicate samples within a single experiment and are representative of three independent experiments. Images in b-c are representative of three independent experiments. Scale bar = 10 μm. *P<0.05.